

# Denoising GNSS Velocities for Earthquake Ground Motions with Deep Learning

Tim Dittmann, *EarthScope Consortium*

Jade Morton, *University of Colorado Boulder*

David Mencin, *EarthScope Consortium*

## BIOGRAPHY

**Dr. Tim Dittmann** is a data scientist at EarthScope Consortium and affiliated researcher at the University of Colorado, Boulder. His research interests include coupling geophysical and remote sensing applications of GNSS with applied data science.

**Dr. Jade Morton** is an Aerospace Engineering Professor at the University of Colorado, Boulder, where she conducts research on satellite navigation technologies and remote sensing of the Earth's ionosphere, atmosphere, and surface. She is a fellow of IEEE, ION, and the Royal Institute of Navigation.

**Dr. David Mencin** is the Director of Data Services at EarthScope Consortium and a Research Scientist at the Cooperative Institute for Research in Environmental Sciences at the University of Colorado Boulder. Dave's current efforts are focused on earthquake and tsunami warning systems and the development and deployment of next generation strainmeters to study earthquake and volcanic processes around the globe.

## ABSTRACT

Distributed measurements of earthquake ground shaking are critical to understanding seismic processes and hazards. High rate, continuous GNSS reference stations are alternative sources of these ground motion observations that complement the dynamic range of traditional inertial-based seismic sensors. GNSS time differenced carrier phase velocity processing (TDCP) has shown to have increased sensitivity to coseismic dynamics when compared to precise point positioning (PPP) while also offering distinct computational advantages. Furthermore, data-driven machine learning (ML) models have proven beneficial for detection and phase picking of seismic waveforms embedded in high-dimensionality noise environments.

In this study, we address this challenging detection problem by modifying existing domain-similar deep learning strategies to take advantage of an established labeled TDCP 5Hz earthquake catalog. We present the results of training a U-net convolutional network architecture used for image processing on denoising temporal windows from a catalog of synthetic 5Hz TDCP waveforms. Unlike traditional fixed bandwidth frequency filtering, the neural network learns a sparse representation mask of time-frequency domain features to separate complex, time-variant noise signatures from a range of signal inputs. These signal inputs from the existing catalog consist of over 2000 observed strong motion velocity waveforms, each augmented with 7 unique noise time series. We use time-frequency domain features from 30 second windows to train a mask on noise-free target waveforms. We report on results of testing denoising unseen synthetic noisy GNSS TDCP time series. We then validate this strategy against both real TDCP waveforms and co-located lower-noise inertial instrumentation.

We find the trained neural network mask filters background noise across a range of time- and spatially-dependent GNSS noise environments. This deep-learned mask permits a spectrum of strong-motion seismic signal signatures to pass through for rapid event characterization and destructive ground motion now-casting. This denoising has the potential to expand the operational role of GNSS in seismic hazard monitoring by increasing signal-to-noise (SNR) of computationally-lightweight TDCP waveforms.

## I. INTRODUCTION

A successful natural hazard monitoring system rapidly learns the severity of the hazard as a function of both time and space. In the event of a significant earthquake, surface ground shaking amplitude and extent are direct observations for quantifying the hazard. Measurements available in real-time can be used for rapid forecasting for warning as well as low-latency now-casting for rapid hazard response. Historically, dedicated inertial-based seismometers are the source of these measurements, directly observing either ground acceleration or velocity at the location of the sensor. Continuously operating, high rate ( $\geq 1\text{Hz}$ ) low-latency GNSS stations provide an additional source of ground motion measurements. These observations are made in a earth-center-of-mass reference frame with virtually no instrumental upper bound or clipping, and so are increasingly valuable observing the nearfield of the largest, most destructive events when traditional seismometers will saturate. Additionally, GNSS ground station networks have spatial distributions to complement inertial sensors, particularly beneficial in regions with sparse instrumentation. However, ground motions estimated from space have elevated noise levels relative to zero-baseline inertial

sensors which limits the contribution of GNSS to operational seismic hazard monitoring and crustal deformation research.

GNSS ground motion sensitivity is largely a function of processing method and signal detection methodology. Regarding the GNSS processing method, the majority of initial GNSS seismology applications focused on precise point positioning (PPP) for earthquake hazards. Numerous experiments have demonstrated that GNSS variometry, or time difference carrier phase (TDCP) processing, is a lightweight processing that is more sensitive to expected ground motions than PPP, at much less computational “cost.” (eg: Colosimo and Mazzoni (2011), Grapenthin et al. (2018), Crowell (2021))

Regarding signal detection amongst noise methodology, traditional GNSS methods were adopted from inertial instruments that are a variation on a threshold or low pass filter. Dittmann et al. (2022) demonstrated that a machine learned classifier trained to identify ground motion events outperformed the traditional state of the art. However, sensitivity is still bounded by relative ambient noise levels, particularly elevated noise levels around the frequencies of seismic signals of interest. Various studies have demonstrated that deep learning architectures can be trained to denoise, or separate signals from noise to remove noise. We present the results of adapting a deep learning architecture from Zhu et al. (2019), later adapted to GNSS PPP displacements by Thomas et al. (2023), to denoise the TDCP velocities. We then explore its implications for operational seismic monitoring.

## II. METHODS

In this work, we evaluate if the synthesis of GNSS processing method, deep learning denoising, and machine learning signal detection increase the sensitivity of GNSS to ground motions for greater operational contributions to hazard monitoring and research analysis.

### 1. TDCP Processing and Catalogs

Our data-driven analysis employs GNSS TDCP or variometric velocity processing for its computational lightweight and increased sensitivity compared to PPP. For a comprehensive description of this processing method, see Grapenthin et al. (2018). In short, TDCP capitalizes on precise GNSS carrier phase measurements by single differencing in time and removing satellite velocity to estimate antenna velocity. Single differencing removes most temporally correlated noise, including the majority of tropospheric, ionospheric and oscillator effects and integer phase ambiguities. A least squares fit of these differenced observables results in direct estimation of antenna velocity and receiver clock drift rate. We emphasize that this method does not estimate absolute position using complex and potentially costly correctional services and processing, but instead estimates precise relative motions, optimal for strong motion recording, with minimal external inputs and computationally efficient.

In this study, we use two TDCP catalogs for training and validation. The first catalog from Dittmann et al. (2022) consists of 1701 5Hz processed TDCP waveforms observed during 77 earthquakes ranging from moment magnitude ( $M_W$ ) 4.8-8.2. This testing catalog includes binary event labels through visual inspection, and also includes over 1500 event-free noise timeseries. The GNSS observables are processed with the SNIVEL software (Crowell (2021), <https://github.com/crowellbw/SNIVEL>), using the narrow-lane phase combination, Niell tropospheric correction, Klobuchar ionospheric correction and broadcast ephemeris. This catalog of real events is used for testing purposes. The second catalog from Dittmann et al. (2023) consists of 2007 inertial strong motion waveforms from 217 events ranging  $M_W$  5.0-7.9, that are downsampled to 5 Hz, superposed on 7 unique noise timeseries and randomly offset. These noise timeseries are generated using a stochastic noise model from observed SNIVEL TDCP ambient velocities. Figure 1 is an example of a single waveform with signal and noise. This much larger augmented dataset supports training data hungry deeper learning models, such as this study, with realistic samples and accurate data labels from a known “truth” in the form of our low-noise inertial based measurements. Data augmentation of these training samples improves the model’s performance extracting signals under varying realistic noise conditions that occur in “real” GNSS variometric velocity timeseries.

### 2. ML Features

We use explicit knowledge of signal and noise components of the synthesized waveforms in the psuedo synthetic augmented catalog to train our neural network. Following the strategy of Zhu et al. (2019) and Thomas et al. (2023), these incoming waveforms,  $Y(t)$  are represented as the superposition of signal  $S(t)$  and noise  $N(t)$ , and their short-time fourier transforms (STFT), can be represented as:

$$Y(t, f) = S(t, f) + N(t, f) \quad (1)$$

Our model input features are the STFT  $Y(t, f)$  from 90 second, non-overlapping windows with 30 sample segments extracted from the horizontal components of motion. We concatenate complex parts of the STFT following the Thomas et al. (2023) result for limiting amplitude distortion. Future work will integrate combined denoising and vertical components. Our model target is a signal mask,  $M_s(t, f)$ :

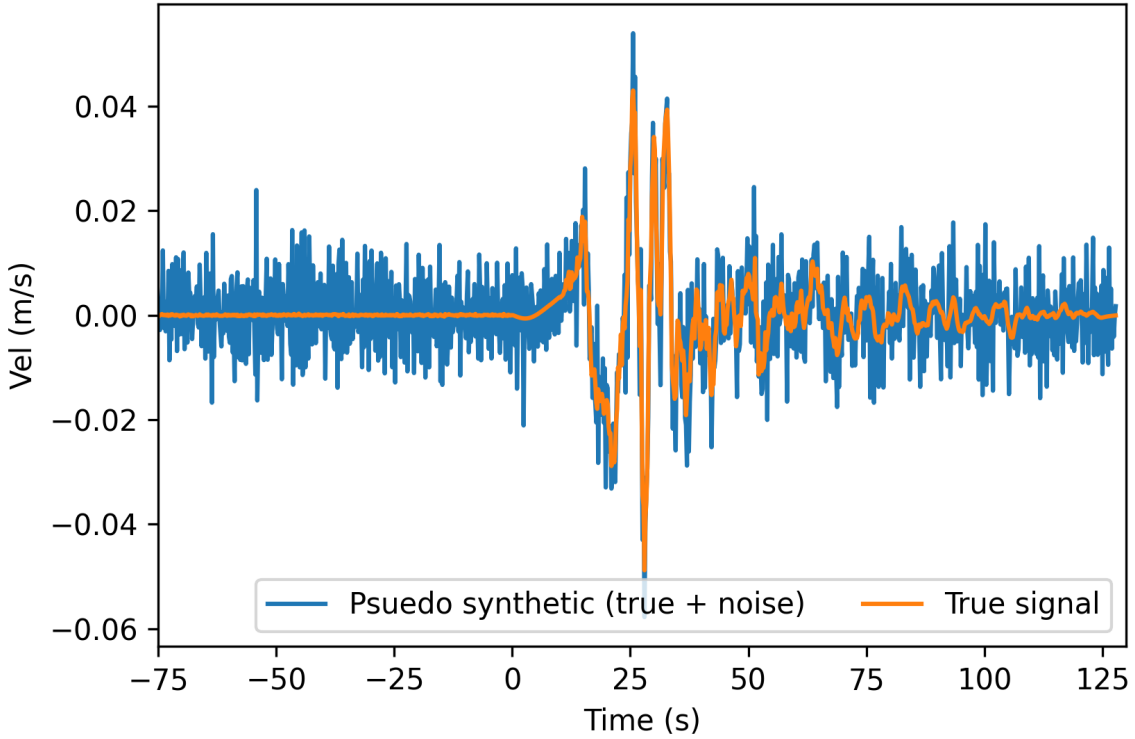


**Figure 1:** An example of a horizontal strong motion waveform from the Kocaeli, Turkey 1999  $M_W$  7.51 strike slip event observed at 55km radius (orange), with synthetic stochastic noise added to the timeseries (blue)

$$M_s(t, f) = \frac{1}{1 + \frac{N(t, f)}{S(t, f)}} \quad (2)$$

where  $N(t, f)$  and  $S(t, f)$  are the noise and signal STFT, respectively. Equation 2 normalizes the target from 0 to 1. We reiterate that it is our explicit knowledge of synthesized timeseries components that makes these targets possible. A denoised STFT is the product of the incoming timeseries and the target signal mask, and the inverse transform,  $TFT^{-1}$  is a resulting denoised timeseries:

$$\hat{S}(t) = TFT^{-1}\{M_s(t, f)Y(t, f)\} \quad (3)$$

This model pipeline is illustrated in Figure 2.

We randomly split the catalog with 80% for training, 10% for validation and 10% for testing. Importantly, we make these splits on discrete seismic events, not individual waveforms or samples. This minimizes information leakage from correlated waveforms to better ensure model generalization for future performance. The resulting dataset for training consists of 74,930 samples of horizontal motion, complex STFTs of dimension 16 x 32. The validation dataset consists of 6,882 samples of complex STFTs.

### 3. Deep Learning Architecture

The convolutional neural network (CNN) employed is a U-Net (Ronneberger et al., 2015) architecture, originally developed for biomedical image-segmentation. This is an efficient deep learning model with a “U” shape that consists of an encoder, or contracting path, for context and a decoder, or expanding path, for context localization (Figure 3). The encoder or downsampling path uses stride 2, doubles the features channels and includes a dropout layer. The decoder path then halves the features in

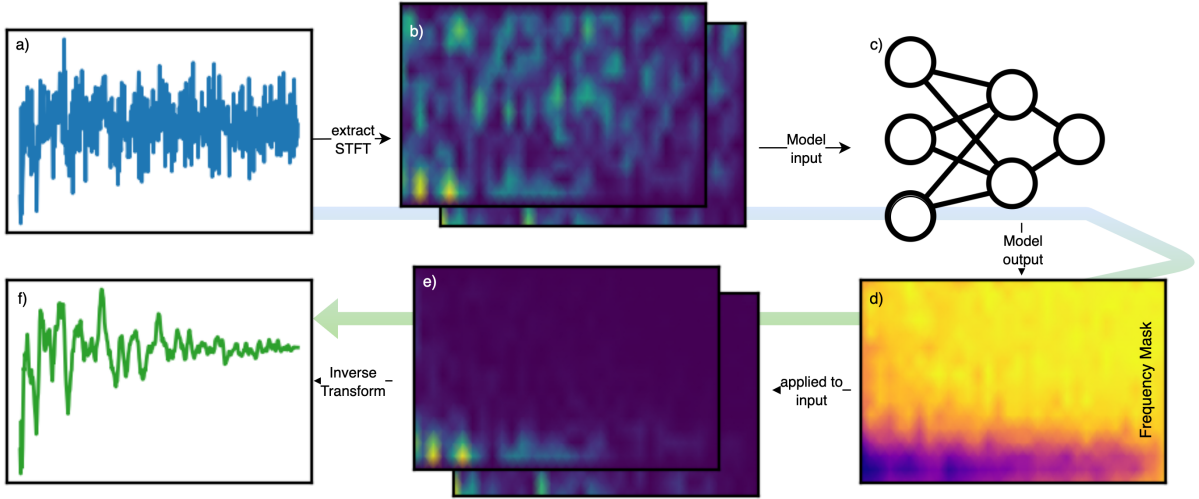


**Figure 2:** Flow chart for denoising GNSS velocities, where a) is a 'raw' single horizontal component 90 second window of 5HZ TDCP velocities. b) is the real and imaginary components of the Short Time Fourier Transform of this incoming (signal+noise) timeseries that are the input to the UNET model, c) (eq: 1). This model outputs a frequency mask, d) (eq: 2), which is then applied to the original inputs, b) to generate a denoised STFT, e). Lastly, the inverse transform (eq: 3) outputs a denoised time series, f).

the "expansive" convolution. Each convolution layer in the model uses rectified linear unit activation function and batch normalization. DeepDenoiser (Zhu et al., 2019) employs such an architecture to learn sparse representation 'images' of inertial sensor waveforms. We adopt a similar strategy later adapted by Thomas et al. (2023), including skip connections for convergence performance in the presence of augmentation.

We train the UNET using the Adam optimizer with a learning rate of 0.001, determined through hyperparameter optimization tuning. The model training is optimized using the mean square estimator (MSE) loss function. We train the model using the open source deep learning software TensorFlow (<https://github.com/tensorflow/tensorflow>), with a batch size of 128 and 50 epochs, determined experimentally. For reference, training runtime for this experiment is approximately 200s per epoch on a AWS ml.g4dn.xlarge instance (4 vCPU, 16GiB Memory).

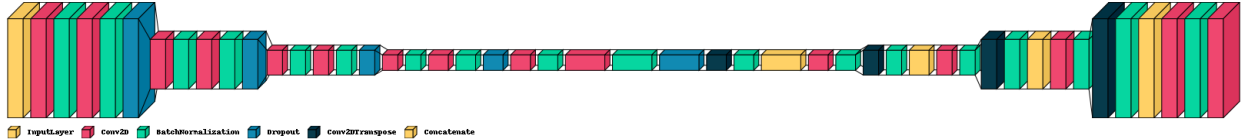


**Figure 3:** Cartoon schematic of the layers of the UNET trained in this experiment. The visualization is generated by the visualkeras software (<https://pypi.org/project/visualkeras/>)

### III. RESULTS AND DISCUSSION

In the training process of the synthetic GNSS waveforms, MSE for the validation set of 6,882 samples is 0.0260. We then evaluate the model on an unseen test set of 13,144 samples, with a MSE of 0.0237. This consistency with unseen data indicates a model that is not overfit. This generalization is then also tested against "real" GNSS observed waveforms in the following:

#### 1. Denoising Performance of Synthetic Testing Data

We provide examples of the model's performance across a range of signatures. Critically, the following examples are from "unseen" testing data from events excluded from model training. Figure 1 illustrates a large signal waveform from a  $M_W$  7.5 at 55km radius (rupture distance). In Figure 4, we demonstrate the denoising performance in the presence of a large, coherent signal. In this context, denoising is likely useful for earlier detection of phase arrivals, but given the amplitude of this signal this effect is likely small. Future work will evaluate detection sensitivity benefits. Figure 5 looks at the trailing end of the incoming surface wave. This relatively weak signal is largely buried in the noise (5 a-0), but denoising (5 c-0) readily extracts

the continuous weaker shaking. While these are not the most destructive phases of the peak dynamics, the ability to observe the duration of shaking of the event from GNSS has implications for hazard monitoring. Interestingly, the PPP model trained in Thomas et al. (2023) struggled to capture these weaker amplitude, later arriving coda waves. Further investigation into the reason for this performance improvement is warranted.

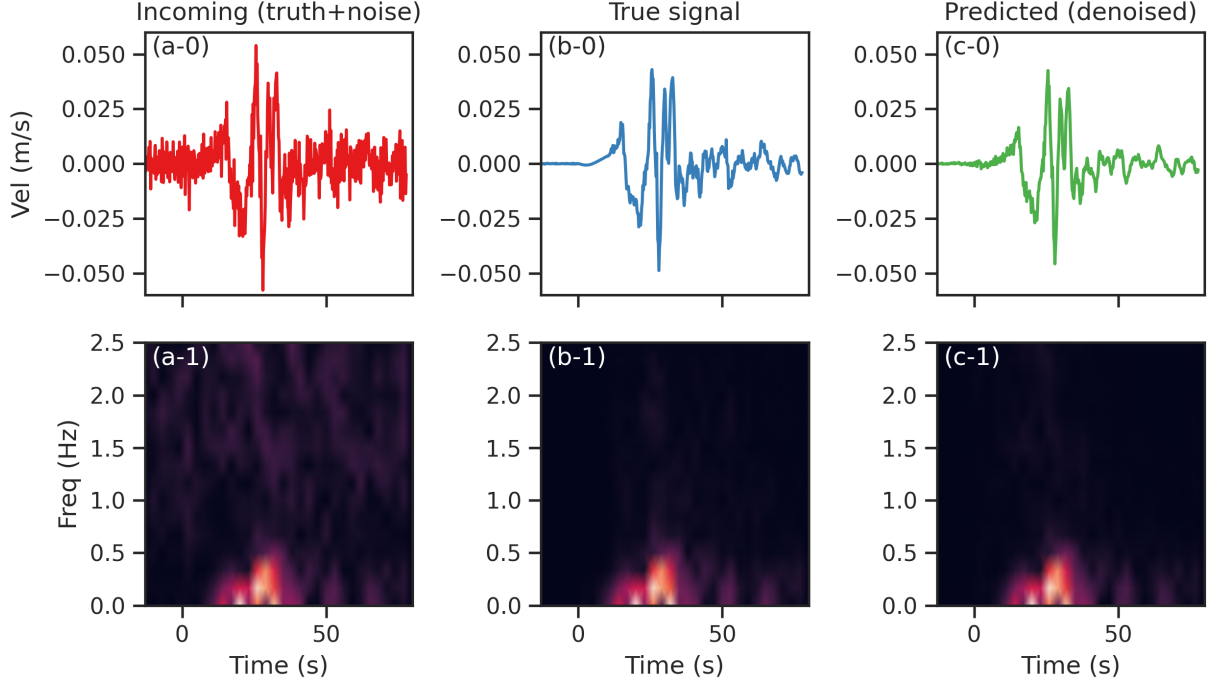


**Figure 4:** A denoised analysis of the early arrival window of a horizontal strong motion waveform from the Kocaeli, Turkey 1999  $M_W$  7.51 strike slip event observed at 55km radius from our testing dataset. The full waveform is in 1. The left panels (a) are the pseudosynthetic waveforms of stochastic GNSS noise (50%) and the true strong motion signal, shown in the middle panels (b). The right panels are the denoised panel (a). The top panels are time series, the bottom panels are the STFT for the window.

We also provide a "weak" signal in this context for further demonstrating the usefulness of denoising. Figure 6 is from a  $M_W$  5.8 in Northern California in 2003 observed at 53Km. Panel (a-0) is the pseudo-synthetic waveform using the 80% noise distribution. At this elevated noise level, the signal is buried in noise in the time domain, and present but not obvious in the STFT domain (a-1). Timing of earliest onset is ambiguous. However, the onset of motion and duration is very apparent denoised waveform (c-0), and the peak amplitudes are in relative agreement. The SNR increase from denoising GNSS TDCP velocities is readily apparent.

We also quantify the difference in SNR between the "raw" incoming GNSS waveforms and the denoised waveforms across the testing dataset (Figure 7). SNR is estimated as follows:

$$SNR(db) = 20 * \log_{10} \frac{\max(|truesignal|)}{2 * \sigma_{noise}} \quad (4)$$

Where  $\max(|truesignal|)$  is the peak amplitude of the noise-free strong motion waveform, and  $\sigma_{noise}$  is the standard deviation of the 30 second window antecedent to the strong motion arrival. The signal portion of this SNR ratio is largely a function of event magnitude and distance from the event, whereas noise is a function of the noise level of the GNSS incoming waveform as well as the level of denoising. On average, denoised waveforms experience an SNR increase from 10db to 50db.

We note that a subset of the denoised waveforms have low SNR. This is apparent in the almost binomial distribution apparent in the marginal kernel density estimate on the right of Figure 7. In Figure 8, we illustrate the increase in SNR by denoising as a function of the peak signal amplitude of the "pure" truth signal waveform. The peak amplitude has a near normal appearing distribution in the x-axis marginal distribution on the top, while the increase in SNR distribution, the marginal of the vertical axis on the right panel, depicts the binomial split. The structure of the density of the sample scatter in Figure 8 suggests that in events observed with a peak amplitude around 0.01 m/s, denoising has a reduced benefit, on average around 10db. At

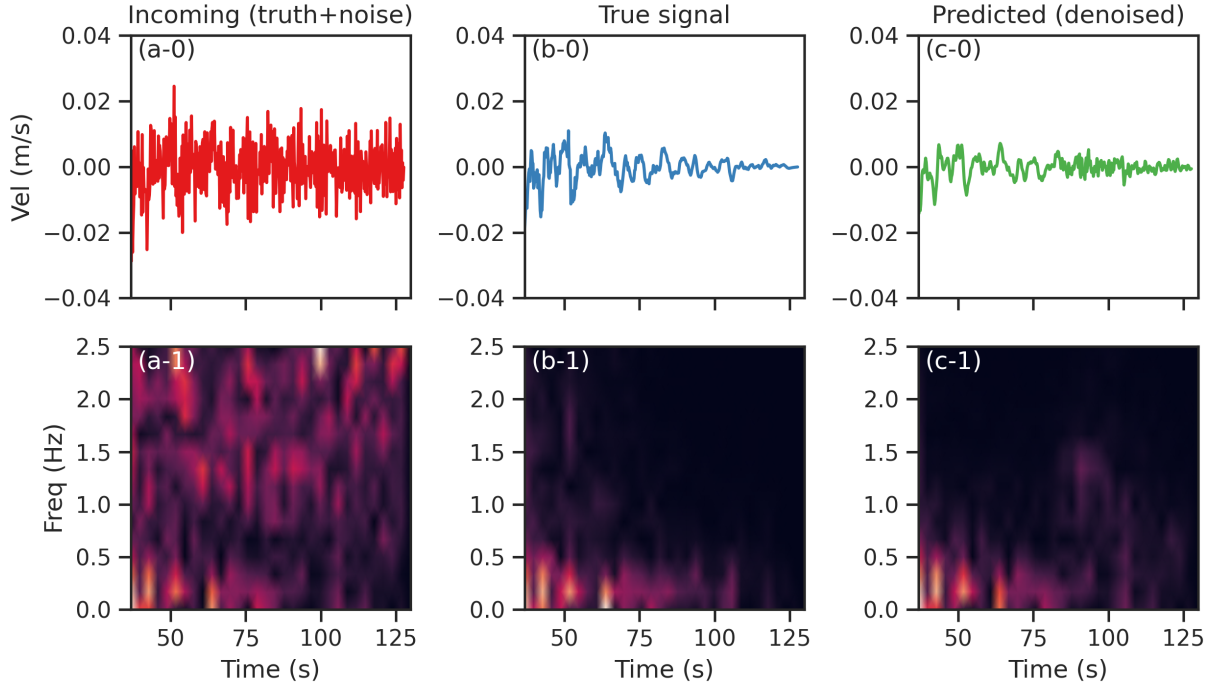


**Figure 5:** A denoised analysis of the later arrival window of a horizontal strong motion waveform from the Kocaeli, Turkey 1999  $M_W$  7.51 strike slip event observed at 55km radius from our testing dataset. The full waveform is 1, and the early window is 4. The left panels (a) are the psuedosynthetic waveforms of stochastic GNSS noise (50%) and the true strong motion signal, shown in the middle panels (b). The right panels are the denoised panel (a). The top panels are time series, the bottom panels are the STFT for the window.

larger amplitudes, denoising almost always has a significant improvement, often greater than 40db. Future investigation into the circumstances that lead to this discrepancy is warranted, particularly with respect to future hazard monitoring implications if not ameliorated.

## 2. Denoising Performance with Real GNSS data

To evaluate the model performance of denoising in a real world scenario, we apply the U-Net model to observed GNSS TDCP waveforms. Future work will evaluate this performance at network scale of the entire catalog spanning 79 events, but we provide some examples of the benefits to more challenging, relatively weak signals.

In Figure 9, we share an observation from the east component at AC20 264km radius from the 2016  $M_W$  7.1 Pedro Bay, Alaska event. Based upon the pre-phase arrival timeseries in panel (a-0), this is a relatively high-noise station, surrounded by significant signal obstruction/multipath vegetation in Girdwood, AK. This location experienced light to moderate shaking (Modified Mercalli Intensity IV-V) in this event, which given the station noise signatures would be difficult to detect given traditional seismic detection methods (e.g. short term average over long term average). The ground motion energy is apparent in the STFT (a-1), but again, difficult to automatically identify, relative to some of the noise signatures present around 20s OT. The arrival of the waveform is clear in the denoised signal (b-0), and earliest phase arrival could readily be extracted by traditional methods. Future investigation into the exact seismic phase and timing, potentially corroborated by nearby inertial instrumentation, would further validate this approach.

Another example of testing and validation of real world GNSS velocity waveforms is shown in Figure 10. In this figure, we compare the east component of motion from station NRWY during the March 2014  $M_W$  4.8 in Yellowstone National Park, to the east component of motion as captured by broadband inertial station YNR. These instruments are within 100's of meters–effectively co-located. The amplitude of this nearly impulse-like signal is sufficiently well above the ambient noise levels of the 'raw' time series in panel (a-0). The denoising decreases noise levels before and after the event, but our primary curiosity is with respect to the peak amplitude of the signal. The difference between GNSS peak ground velocity ( 0.19 m/s), denoised GNSS ( 0.18 m/s) and the broadband instrument ( 0.1 m/s) is significant. The amplitude difference is much greater than typical noise levels, and so seems unlikely to be the only source of difference. Hyperlocal site effects, aliasing, and instrumentation

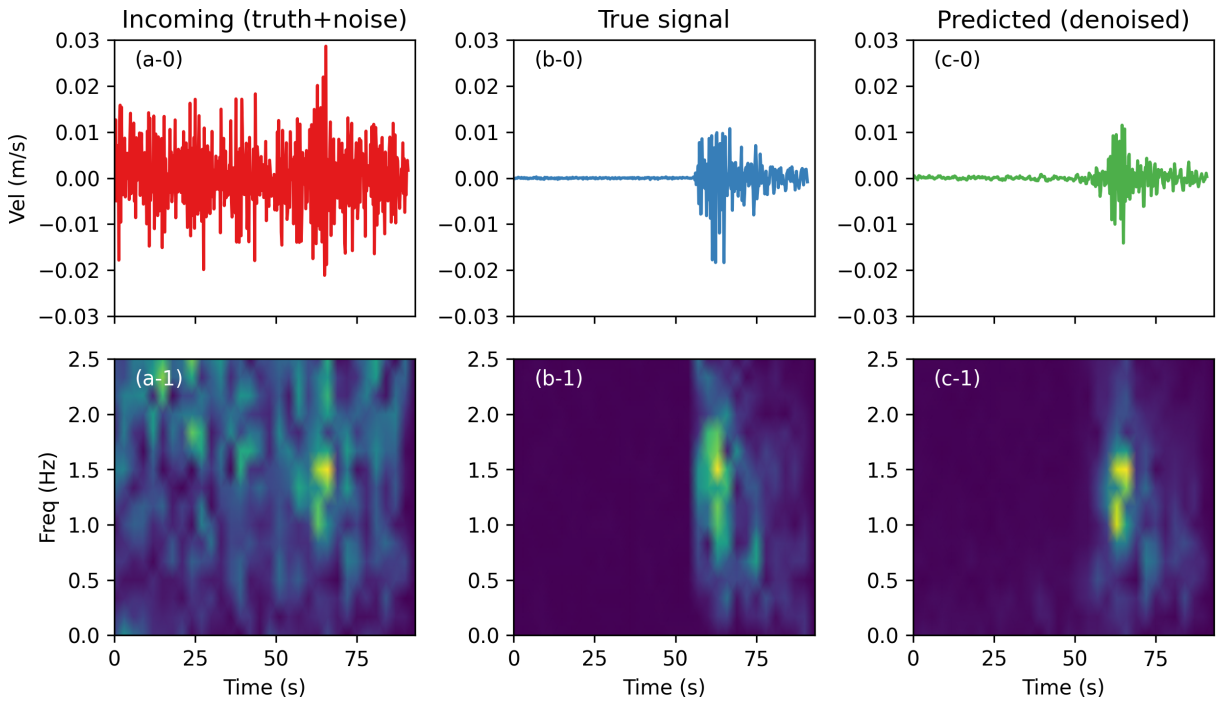


**Figure 6:** A denoised analysis of a horizontal strong motion waveform from the 2003 NW California  $M_w 5.8$  event observed at 53km radius from our testing dataset. The left panels (a) are the pseudosynthetic waveforms of stochastic GNSS noise (80%) and the true strong motion signal, shown in the middle panels (b). The right panels are the denoised panel (a). The top panels are time series, the bottom panels are the STFT for the window.

responses are possible scenarios for these differences, and illustrate some of the potential challenges with validation of sensors seemingly measuring the "same" signals at the "same" place and time.

#### IV. CONCLUSIONS

In this experiment, we evaluated the performance of a deep learning denoising model trained on a large catalog of augmented pseudo synthetic GNSS velocity strong motion waveforms. The U-Net model is able to learn a sparse representation mask of time-frequency domain features. We found significant SNR enhancement of our test dataset synthetic waveforms when denoised, often close to 40db. Future investigations should inspect the model's performance as a function of additional event and instrumentation parameters, including addressing the binomial subset of the  $\Delta$ SNR distribution that experienced less denoising. We provide anecdotal evidence of the model's performance with real GNSS event waveforms, but future work will comprehensively address real-world benefits, particularly with respect to detectability and dynamic response accuracy for real-time seismic monitoring and earthquake source characterization, and mitigation of non-seismic 'noise' events. These preliminary results suggest that this substantial SNR enhancement of real-GNSS signals would yet further expand the range of valid GNSS contributions to the broader seismic infrastructure. Future development coupling real-time ML-driven denoising and signal detection in operational streaming pipelines of lightweight, high rate GNSS TDCP processing is a scalable and sustainable MLOps architecture for next generation GNSS seismology monitoring for contributing to the global seismic infrastructure.

#### ACKNOWLEDGEMENTS

This material is based on services provided by the GAGE Facility, operated by EarthScope, Inc., with support from the National Science Foundation, the National Aeronautics and Space Administration, and the U.S. Geological Survey under NSF Cooperative Agreement EAR-1724794. High-rate processing and machine learning for geoscience and hazards research is supported by NSF OAC-1835791.

This experiment and manuscript are made possible by open source software, in particular SNIVEL, TensorFlow, Pandas, and Obspy, open science (<https://github.com/AI4EPS/DeepDenoiser>, [https://github.com/amtseismo/hrgnss\\_](https://github.com/amtseismo/hrgnss_)

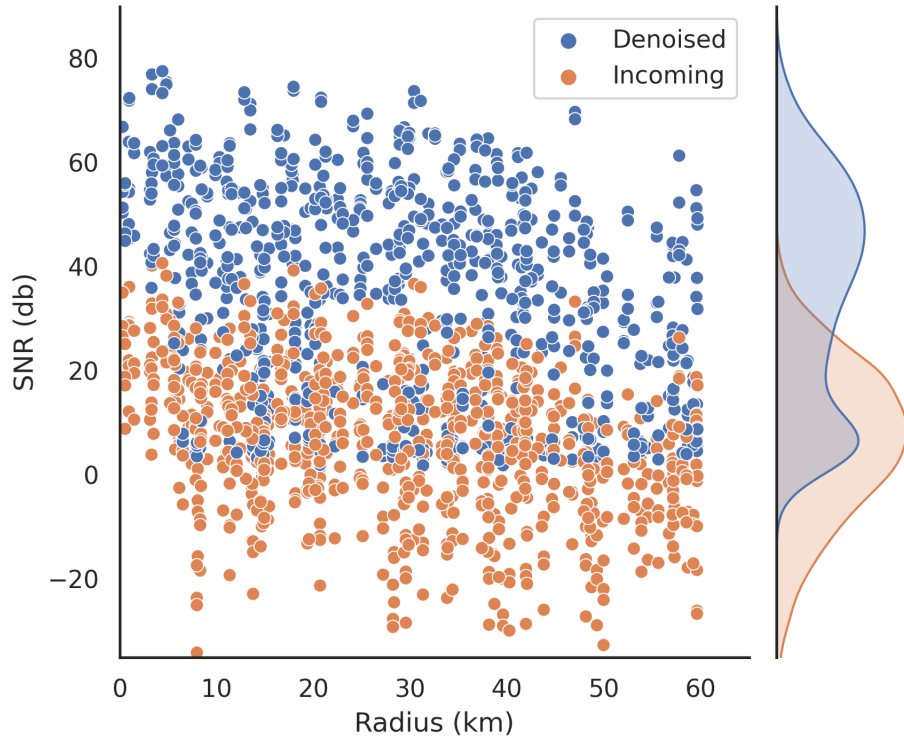


**Figure 7:** Comparison of SNR (equation 4) as a function of radius for "Incoming" pseudosynthetic TDCP velocity waveforms (blue) and their denoised version (orange). The right panel is a kernel density estimate of the distribution as a function of SNR. Waveforms included in this analysis are all of the testing dataset for every other noise level (5, 35, 65, 95 percentiles)

denoising, open labeled datasets (<https://zenodo.org/records/7909327>) and open archives ([www.earthscope.org](http://www.earthscope.org), <https://peer.berkeley.edu/research/nga-west-2>).

## REFERENCES

- Colosimo, G., M. C. and Mazzoni, A. (2011). Real-time gps seismology with a stand-alone receiver: A preliminary feasibility demonstration. *Journal of Geophysical Research*, 116(B11302).
- Crowell, B. W. (2021). Near-field strong ground motions from gps-derived velocities for 2020 intermountain western united states earthquakes. *Seismol. Res. Lett.*, XX(1-9).
- Dittmann, T., Liu, Y., Morton, Y., and Mencin, D. (2022). Supervised Machine Learning of High Rate GNSS Velocities for Earthquake Strong Motion Signals. *Journal of Geophysical Research: Solid Earth*, 127(11).
- Dittmann, T., Morton, Y. J., Crowell, B., Melgar, D., DeGrande, J., and Mencin, D. (2023). Characterizing high rate gnss velocity noise for synthesizing a gnss strong motion learning catalog. *Seismica*, 2(2).
- Grapenthin, R., West, M., Tape, C., Gardiner, M., , and Freymueller, J. (2018). Single-frequency instantaneous gnss velocities resolve dynamic ground motion of the 2016 mw 7.1 iniskin, alaska, earthquake. *Seismol. Res. Lett.*, 89(1040-1048).
- Ronneberger, O., Fischer, P., and Brox, T. (2015). U-net: Convolutional networks for biomedical image segmentation.

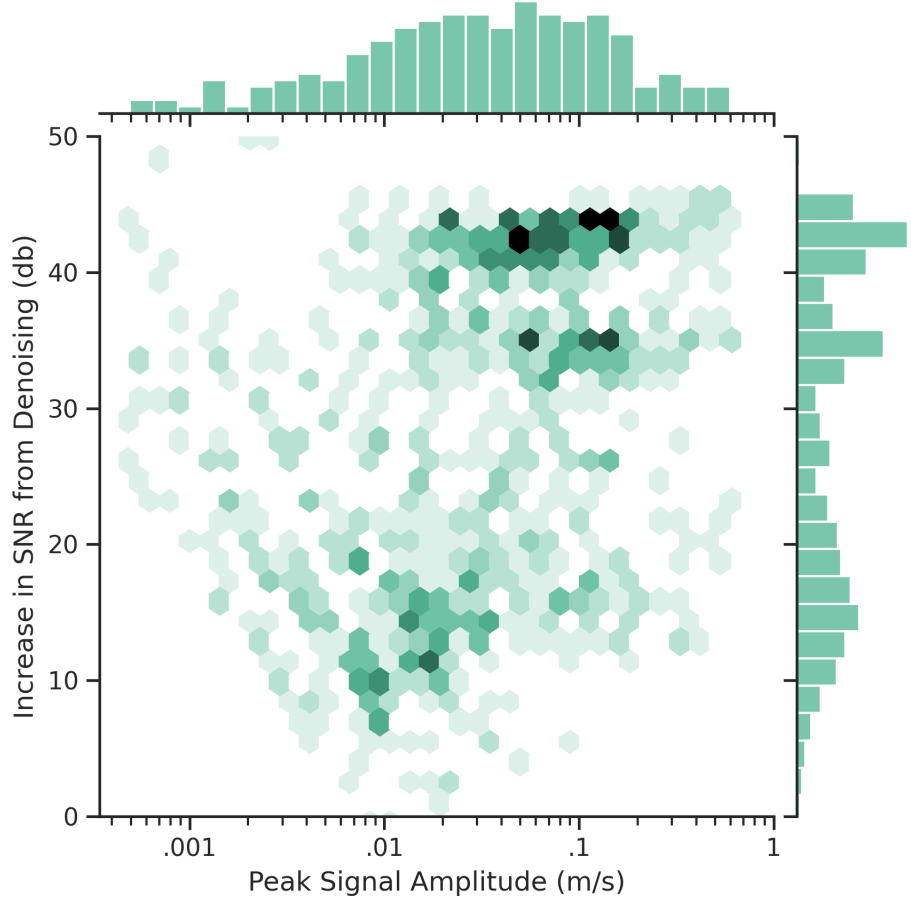


**Figure 8:** Distribution of Increase in SNR from Denoising ( $SNR_{denoised} - SNR_{incoming}$ ) as a function of peak signal amplitude. The scatter is shaded by density of samples, and the marginal distributions for signal amplitude and SNR increase are visible on the top and right panels, respectively

Thomas, A., Melgar, D., Dybing, S. N., and Searcy, J. R. (2023). Deep learning for denoising high-rate global navigation satellite system data. *Seismica*, 2(1).

Zhu, W., Mousavi, S. M., and Beroza, G. C. (2019). Seismic signal denoising and decomposition using deep neural networks. *IEEE Transactions on Geoscience and Remote Sensing*, 57(11):9476–9488.

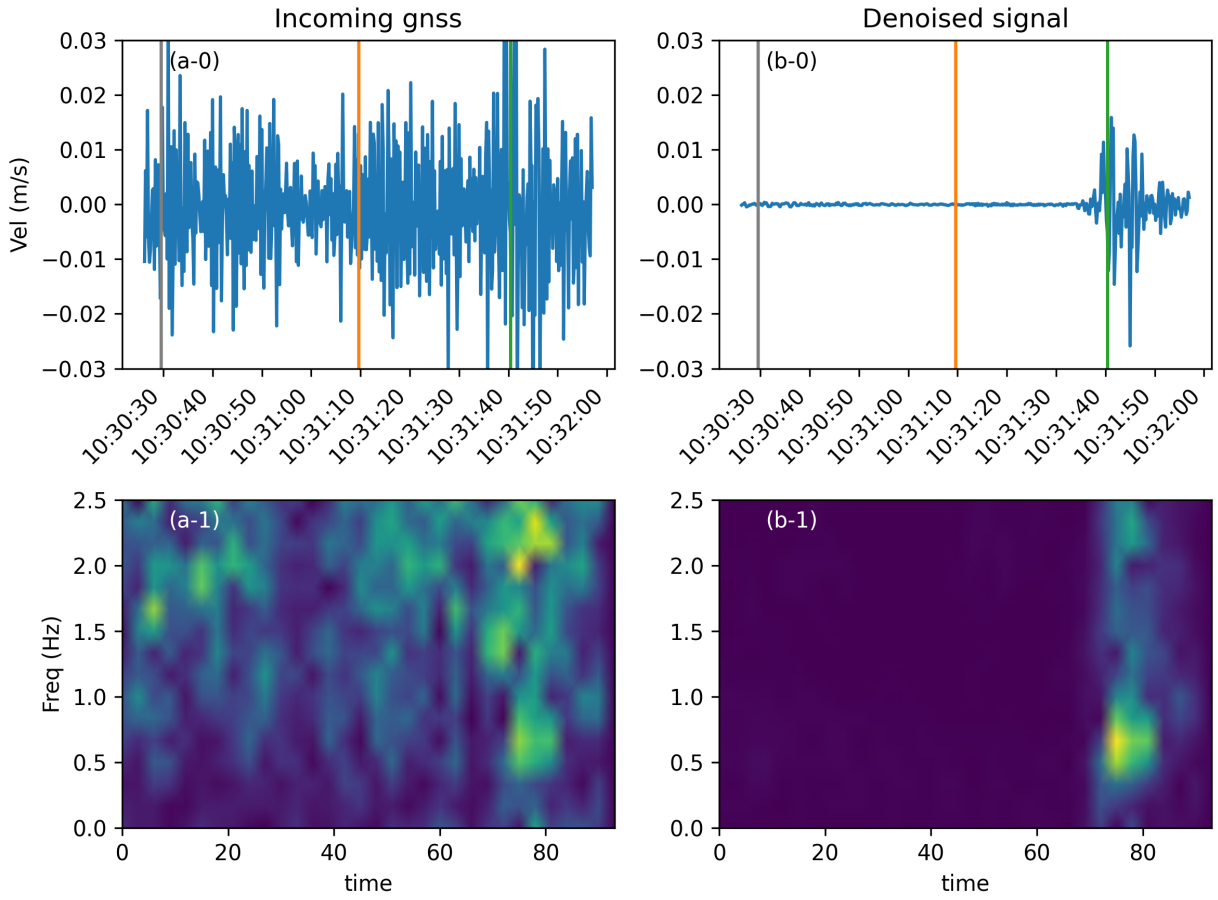


**Figure 9:** Panel a-0 is the east component of velocity observed GNSS station AC20 264km radius from the 2016  $M_W$  7.1 Pedro Bay, Alaska event. (b-0) is the denoised timeseries derived from applying panel a-0 to the U-Net model. Gray lines are the origin time, and red and green are the p- and s-wave expected arrival times, respectively, given an IASP91 1-D velocity model. Bottom panels are the STFT of the respective time series

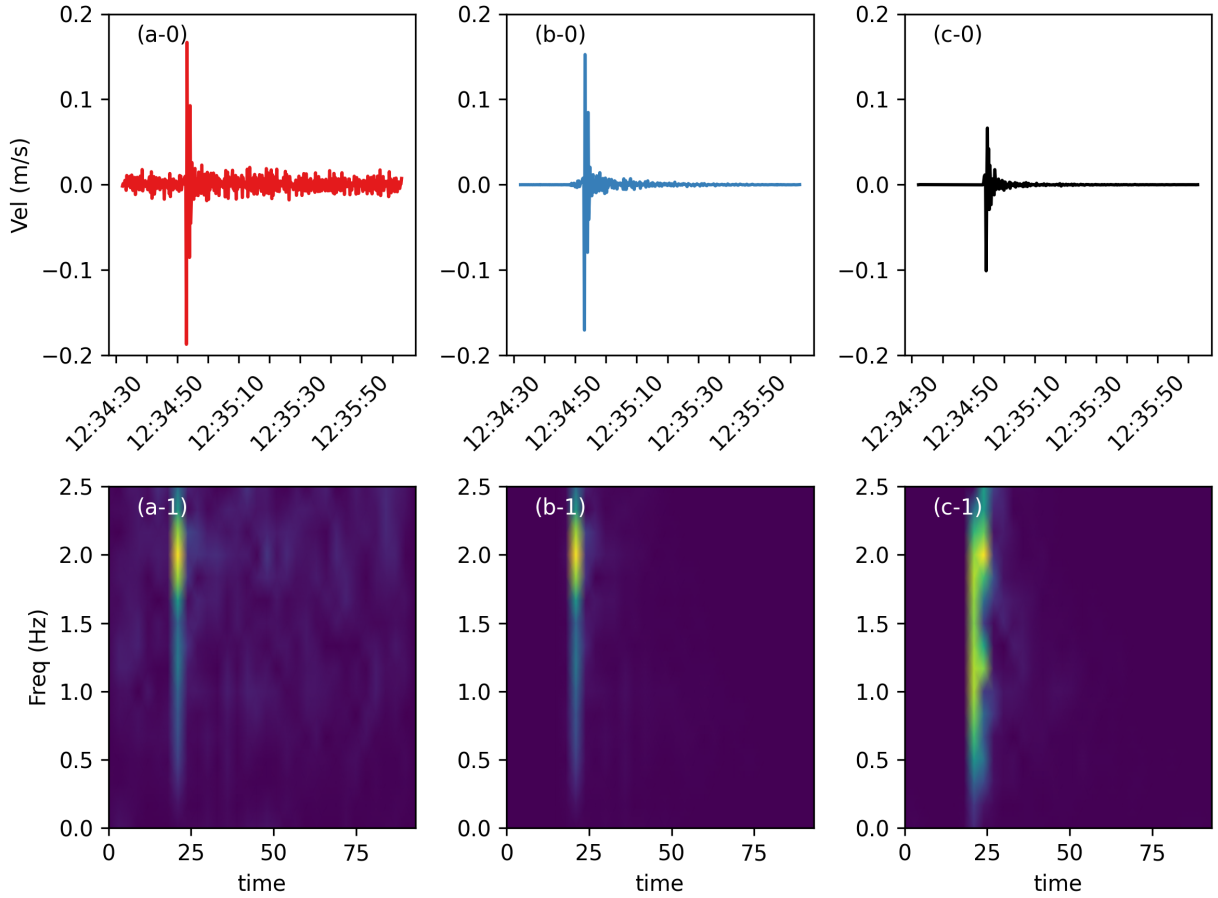


**Figure 10:** Comparing the TDCP observed during a M4.8 30 March 2014 at GPS station NRWY (a), with a denoised version (b) and a co-located broadband instrument YNR in network WY in Yellowstone National Park (c). The bottom panels are the concurrent STFT images